Atmos. Meas. Tech. Discuss., 5, 589–625, 2012
www.atmos-meas-tech-discuss.net/5/589/2012/
doi:10.5194/amtd-5-589-2012
© Author(s) 2012. CC Attribution 3.0 License.

Atmospheric Measurement Techniques Discussions

This discussion paper is/has been under review for the journal Atmospheric Measurement Techniques (AMT). Please refer to the corresponding final paper in AMT if available.

Multi-wavelength Raman lidar, sunphotometric and aircraft measurements in combination with inversion models for the estimation of the aerosol optical and physico-chemical properties over Athens, Greece

R. E. Mamouri[1], A. Papayannis[1], V. Amiridis[2], D. Müller[3,4], P. Kokkalis[1], S. Rapsomanikis[5], E. T. Karageorgos[5], G. Tsaknakis[1], A. Nenes[6,7], S. Kazadzis[8], and E. Remoundaki[9]

[1]National Technical University of Athens, Laser Remote Sensing Laboratory, Athens, Greece
[2]Nat. Obs. of Athens, Institute for Space Applications and Remote Sensing, Athens, Greece
[3]Leibniz Institute for Tropospheric Research, Leipzig, Germany
[4]Atmospheric Remote Sensing Laboratory, Gwangju Institute of Science and Technology, Department of Environmental Science and Engineering, Gwangju, South Korea
[5]Democritus Univ. Thrace, Department of Environmental Engineering, Xanthi, Greece

[6]Georgia Inst. of Techn., School of Earth and Atm. Sc. and Chem. & Biomolecular Engineering, Atlanta, GA, USA
[7]Institute of Chemical Engineering and High-Temperature Chemical Processes, Foundation for Research and Technology Hellas, Patras, Greece
[8]Institute for Environmental Research and Sustainable Development, National Observatory of Athens, I. Metaxa and Vas. Pavlou, 15236, P. Penteli, Athens, Greece
[9]National Technical University of Athens, School of Mining and Metallurgical Engineering, Zografou, Greece

Received: 29 December 2011 – Accepted: 6 January 2012 – Published: 13 January 2012

Correspondence to: A. Papayannis (apdlidar@central.ntua.gr)

Published by Copernicus Publications on behalf of the European Geosciences Union.

Abstract

A novel procedure has been developed to retrieve, simultaneously, the optical, microphysical and chemical properties of tropospheric aerosols with a multi-wavelength Raman lidar system in the troposphere over an urban site (Athens, Greece: 37.9° N, 23.6° E, 200 m a.s.l.) using data obtained during the European Space Agency (ESA) THERMOPOLIS project which took place between 15–31 July 2009 over the Greater Athens Area (GAA). We selected to apply our procedure for a case study of intense aerosol layers occurred on 20–21 July 2009. The National Technical University of Athens (NTUA) EOLE 6-wavelength Raman lidar system has been used to provide the vertical profiles of the optical properties of aerosols (extinction and backscatter coefficients, lidar ratio) and the water vapor mixing ratio. An inversion algorithm was used to derive the mean aerosol microphysical properties (mean effective radius – r_{eff}), single-scattering albedo (ω) and mean complex refractive index (m) at selected heights in the 2–3 km height region. We found that r_{eff} was 0.3–0.4 μm, ω at 532 nm ranged from 0.63 to 0.88 and m ranged from $1.45 + 0.015i$ to $1.56 + 0.05i$, in good accordance with in situ aircraft measurements. The final data set of the aerosol microphysical properties along with the water vapor and temperature profiles were incorporated into the ISORROPIA model to infer an in situ aerosol composition consistent with the retrieved m and ω values. The retrieved aerosol chemical composition in the 2–3 km height region gave a variable range of sulfate (0–60 %) and organic carbon (OC) content (0–50 %), although the OC content increased (up to 50 %) and the sulfate content dropped (up to 30 %) around 3 km height; in connection with the retrieved low ω value (0.63), indicates the presence of absorbing biomass burning smoke mixed with urban haze. Finally, the retrieved aerosol microphysical properties were compared with column-integrated sunphotometer data.

1 Introduction

Atmospheric aerosols have large influence on Earth's radiation budget. Recent estimations on the possible impact of aerosols (both direct and indirect effects) on the radiative forcing (cooling effect) in a global average show that they may be of the same order of magnitude as the CO_2 effect (warming effect) (Kirkevag et al., 2008; Quaas et al., 2009; Ramanathan and Feng, 2009; Lohmann et al., 2010; Rapsomanikis et al., 2011), in addition to having direct impact on precipitation (Levin and Cotton, 2009; Lee, 2011; Wulfmeyer et al., 2011). However, medium to high uncertainties still exist concerning the indirect and direct effects, which are connected with the aerosol influence on climate. Moreover, the total direct aerosol radiative forcing combined across all aerosol types is $-0.5\,\text{Wm}^{-2}$, with a 5 to 95 % confidence range of -0.1 to $-0.9\,\text{Wm}^{-2}$ (IPCC, 2007) and with a medium-low level of scientific understanding. This is especially true for the Eastern Mediterranean region (Stock et al., 2011), where a sufficient knowledge of the microphysical properties of aerosol particles as well as their spatial distribution remains a unknown key-issue to evaluate their effect on global climate.

Therefore, experimental data, in our area are strongly needed as input parameters for global climate models, which assess the role of aerosols in future scenarios of Global Change. Currently, very little is known about the vertical distribution of the aerosol microphysical properties in the Eastern Mediterranean region in connection to the air quality impairment (Formenti et al., 2002; Dulac and Chazette, 2003; Papayannis et al., 2011). Furthermore, knowledge on the combined optical-microphysical-chemical properties of free-tropospheric aerosol particles of different origin (i.e. Saharan dust, forest fires and urban activities, long-range transported, etc.) over Greece is particularly sparse, at least in the vertical scale (Papayannis et al., 2010, 2011). However, several in situ aerosol sampling in urban areas of Greece has revealed that coarse aerosols in the city of Athens usually contain predominant ions such as Ca_2^+, NO_3^-, Na^+ and Cl^- while SO_4^{2-}, Ca_2^+ and NH_4^+ were the major ionic components of the fine fraction (Karageorgos and Rapsomanikis, 2007), aluminosilicates, and also

calcium which was distributed between calcite, dolomite, gypsum and Ca-Si particles mostly observed during Saharan dust outbreaks (Remoundaki et al., 2011).

The Raman laser remote sensing technique is a unique tool able to provide the vertical distribution of the aerosol optical properties (aerosol backscattering and extinction coefficients, lidar ratio-LR) and the water vapor content, expressed in terms of mixing ratio of water vapor in dry air (Bösenberg et al., 2003; Böckmann et al., 2004; Weitkmap, 2005; Mamouri et al., 2007; Papayannis et al., 2005). It is well known that, when multi-wavelength lidar data are used, the main microphysical aerosol properties can be obtained using inversion techniques (Müller et al., 1999a,b; Veselovskii et al., 2001; Osterloh et al., 2011). Our work goes a further step on: using a novel procedure it combines 6-wavelength Raman lidar data, inversion models and an aerosol thermodynamic model to retrieve simultaneously the vertical profiles of optical, microphysical and chemical properties of aerosol particles, consistent with the retrieved refractive index and single scattering albedo values. These results are then compared to airborne in situ data obtained in the frame of the European Space Agency (ESA) THERMOPOLIS research project carried out between 15 and 31 July 2009.

Section 2 of this paper presents the methodology applied and the instrumentation involved; we first give a short description of the National Technical University of Athens (NTUA) Raman lidar system (range-resolved measurements) and the CIMEL sun photometer (columnar measurements) used for the retrieval of the aerosol optical and microphysical properties. The third part of this section provides the characteristics of the in situ (airborne) instrumentation used to measure the aerosol optical and microphysical properties. The fourth part of this section gives a short description of the inversion models to retrieve the aerosol microphysical and chemical properties. Section 3 gives a short description of the THERMOPOLIS campaign, while Sect. 4 presents a case study analysis where we compare the retrieved with the in situ measured aerosol optical and microphysical properties, as well as the estimated aerosol chemical composition a loft. Finally, Sect. 5 presents summary and concluding remarks.

2 Methodology and experimental set up

2.1 Raman lidar system for the retrieval of the aerosol optical properties

At NTUA a compact 6-wavelength Raman lidar system (EOLE) is used to perform continuous measurements of suspended aerosols particles in the Planetary Boundary Layer (PBL) and the lower troposphere. The system is based on a pulsed Nd:YAG laser emitting simultaneously at 355, 532 and 1064 nm. The respective emitted output energies per pulse are 75, 130 and 140 mJ, with a 10 Hz repetition rate. The optical receiver is a Cassegrainian reflecting telescope with a primary mirror of 300 mm diameter and a focal length of $f = 600$ mm, directly coupled, through an optical fiber, to the lidar signal six-channel filter spectrometer. The full overlap of the system is of the order of 500 m. The elastically backscattered lidar signals (at 355, 532 and 1064 nm), as well as those generated by Raman scattering by atmospheric N_2 and H_2O (at 387, 607 and 407 nm, respectively) are simultaneously recorded by photomultipliers (PMTs) and avalanche photodiode systems (APD), after the spectral separation of the returned lidar signals. The lidar signals detected at 355, 387, 532, 607 and 1064 nm were used to derive the aerosol backscatter (at 355, 532 and 1064 nm), the extinction (at 355 and 532 nm) coefficient and the Ångström exponent profiles, while the 407 nm channel was used to derive the water vapor mixing ratio (Mamouri et al., 2007). The NTUA lidar system has been quality-assured by performing direct inter-comparisons, both at hardware (Matthias et al., 2004a) and software levels (Böckmann et al., 2004; Pappalardo et al., 2004).

More precisely, to obtain reliable and quantitative lidar aerosol retrievals, several techniques and methods have to be combined. The standard backscatter lidar technique is appropriate to retrieve aerosol parameters mostly for small aerosol optical depths (AOD) (AOD < 0.2–0.3 in the visible), assuming a reference height in an aerosol-free region (e.g. the upper troposphere). Under such conditions, the Klett inversion technique (Klett, 1985) is used to retrieve the vertical profile of the aerosol backscatter coefficient (b_{aer}) at the respective wavelengths. The resulting average

uncertainty on the retrieved b_{aer} values (including both statistical and systematic errors corresponding to a 30–60 min averaging time) in the troposphere is of the order of 20–30 % (Bösenberg et al., 1997). To overcome the large uncertainty associated with this technique, the Raman N_2 lidar technique was adopted using the methodology of Ansmann et al. (1992). Since the Raman lidar signals are quite weak, the Raman technique is mostly used during nighttime, when the atmospheric background is rather low. In the case of the Raman technique, the measurement of the elastic backscatter signals at 355 and 532 nm, as well as that of the N_2 inelastic-backscatter signals at 387 and 607 nm, respectively, permits the determination of the aerosol extinction (a_{aer}) and b_{aer} coefficients independently of each other (Ansmann et al., 1992) and, thus, of the extinction-to-backscatter ratio, the so-called lidar ratio (LR) at both wavelengths (355 and 532 nm). The uncertainties associated with the retrieved a_{aer} and b_{aer} vertical profiles are of the order of 10–25 % and 5–15 %, respectively (Ansmann et al., 1992; Mattis et al., 2002). The vertical profiles of b_{aer} referring to measurements performed before the local sunset time (around 19:00 UT) were retrieved by using the Klett technique, using a LR value derived for dust aerosols by the Raman technique (Ansmann et al., 1992) from the same day's nighttime lidar measurements.

2.2 The CIMEL sunphotometer

The sunphotometric observations reported in this paper were performed by a CIMEL sun-sky radiometer (Holben et al., 1998), which is part of the Aerosol Robotic Network (AERONET) Global Network (http://aeronet.gsfc.nasa.gov). The instrument is located on the roof of the Research Center for Atmospheric Physics and Climatology of the Academy of Athens (37.99° N, 23.78° E, elevation: 130 m). The site is located in the outskirts of Athens, 1.5 km from the NTUA Raman lidar and about 10 km from the sea. This sunphotometric station is operated by the Institute for Space Applications and Remote Sensing (ISARS) of the National Observatory of Athens (NOA). The CIMEL data used in this study will provide information about the columnar AOD, the aerosol size distribution (ASD), and finally, the Ångström exponent (*å*). The AERONET data

products along with the technical specifications of the CIMEL instrument are given in detail in Holben et al. (1998).

2.3 In situ (airborne) aerosol measurements: instrumentation and methodology

The airborne measurements of the THERMOPOLIS campaign were carried out with the modified "Cessna 310" aircraft of the Democritus University of Thrace. Both the instrumentation and methodology are described in detail elsewhere (Rapsomanikis et al., 2011), therefore only a short description will be provided below. The size-distribution of the aerosols was determined using an Optical Particle Counter (hereafter referred to as OPC, PMS Systems, Lasair 5295), in 8 diameter ranges (bins) corresponding to the aerodynamic diameters of 0.3–0.5, 0.5–1, 1–2, 2–3, 3–5, 5–10, 10–25, >25 µm. Aerosol scattering coefficient measurements were carried out using a model M903 integrating nephelometer (Radiance Research Operation, Seattle, USA) measuring at 530 nm and at 1 Hz. The aerosol light absorption coefficient was also determined at 1 Hz and at 565 nm, by means of a Radiance Research filter-based Particle Soot/Absorption Photometer. The data from the PSAP were corrected according to Bond et al. (1999). A GPSMAP 195 (Garmin International Inv, USA) was used in order to provide 3-dimensional location information (latitude, longitude, altitude, World Geodetic System 84) of the aircraft at 1 Hz sampling frequency. The particle mean effective radius (r_{eff}) (Wyser, 1998) was calculated using the particle size-distribution obtained with the above-mentioned OPC. The "fine" fraction r_{eff} corresponds to the smallest size bin, while the "total" refers to particles up to 5 µm in diameter. The values of the single-scattering albedo (ω) (Goody, 1996) were derived using concurrently obtained values for the optical extinction coefficient for absorption and the light scattering extinction coefficient, obtained with the PSAP and the nephelometer, respectively.

2.4 Retrieval of the microphysical and chemical aerosol properties profiles using models

The microphysical particle properties of the spherical aerosols inside various layers in the lower free troposphere, were retrieved using the hybrid regularization technique. A detailed description of the original version of the algorithm which assumes spherical shape of the investigated particles in the retrieval procedures given by Müller et al. (1999a,b). Modifications concerning the optimum solution space were made by Veselovskii et al. (2001, 2002, 2005). Changes concerning the minimum number of the needed measured wavelengths can be found in Müller et al. (2001). These models use as input the mean values of the optical properties of the aerosols calculated from the vertical profiles of elastic and Raman backscattered lidar signals (obtained at 5 different wavelengths: 355-387-532-607-1064 nm). The aerosol microphysical properties which were derived are the r_{eff}, as well as ω and the mean complex refractive index (m).

The inverted refractive index along with the water vapor profiles obtained by Raman lidar over Athens and the temperature and relative humidity profiles obtained by radiosonde, were incorporated in the thermodynamic model ISORROPIA II (Fountoukis and Nenes, 2007) to infer the particle chemical composition. The model treats the thermodynamics of aerosol containing K, Ca, Mg, NH_3/NH_4, Na, SO_4/HSO_4, HNO_3/NO_3, HCl/Cl and H_2O. ISORROPIA-II can predict composition for the "stable" (or deliquescent path) solution where salts precipitate once the aqueous phase becomes saturated with respect to a salt, and, a "metastable" solution, where the aerosol is composed only of an aqueous phase regardless of its saturation state. ISORROPIA-II was executed in "reverse" mode, where known quantities are T , RH and the concentrations of aerosol K, Ca, Mg, NH_4, Na, SO_4, NO_3 and Cl. The output provided by ISORROPIA-II is the aerosol phase state (solid only, solid/aqueous mixture or aqueous only) and the speciation in the gas and aerosol phases. The model has been evaluated with ambient data from a wide range of environments (Moya et al., 2001; Zhang et al., 2003;

San Martini et al., 2006; Nowak et al., 2006; Metzger et al., 2006; Fountoukis et al., 2009), while its computational rigor and performance makes it suitable for use in large scale air quality and chemical transport models. Some examples of such 3-D models that have implemented ISORROPIA-II are GISS, CMAQ, $PMCAM_x$, GEOS-Chem, and ECHAM/MESSy (Adams and Seinfeld, 2002; Yu et al., 2005; Pye et al., 2009; Karydis et al., 2010; Pringle et al., 2010).

In order to use ISORROPIA in combination with the Raman lidar data, an assumption concerning the aerosol composition has to be done, mainly due to the absence of air mass sample within the under study layers. In our procedure, at first a typical composition of sulfate, ammonium sulfate and mineral dust aerosols was considered. ISORROPIA was run forward for the computation of complex refractive index for each aerosol composition, using as input the relative humidity and the temperature within an aerosol layer. Finally, the aerosol composition (a mixture of sulfate, ammonium and mineral dust) with the closest refractive index (both real and imaginary part) value to the one estimated by the inversion model is provided as the most acceptable composition value.

3 The THERMOPOLIS campaign

In the framework of its Earth Observation Programs, the European Space Agency (ESA) carries out a number of ground-based and airborne campaigns to support the geophysical algorithm development, calibration/validation and the simulation of future space-borne earth observation missions for applications development related to land, oceans and atmosphere. The THERMOPOLIS 2009 campaign (Daglis et al., 2010) was part of the framework of proposed activities for the "Urban Heat islands (UHI) and Urban Thermography (UT) Project" for Athens, Greece. This campaign combined the collection of quality and coordinated airborne hyper-spectral, space-borne and in-situ measurements to generate spectrally, geometrically and radiometrically representative

datasets to address observational requirements of UHI for the assessment of an operational system.

The period 15 to 31 July 2009 was an optimal time window with fair weather conditions prevailing over Athens, where the campaign was carried out. The core measurement period for the ground-based instrumentation was in 15–27 July 2009. During the campaign the aerosol load presented a large variation connected with different meteorological conditions, due to advected air masses from different origins. More precisely, the mean value of AOD (crosses) measured by the CIMEL varied between 0.07 and 0.35 at 500 nm, while that of the Ångström exponent ($å$ – 440/870 nm) (triangles) was found between 0.75 and 1.75 (Fig. 1, upper panel).

In order to estimate the free tropospheric contribution of the particles, the AODs at 532 nm obtained by the Raman lidar extinction profiles for 17–25 July 2009 (Fig. 1, bottom panel), were calculated in the height range below (squares) and above 2 km (open dots), which is the mean PBL height for July over Athens (Matthias et al., 2004b). From this figure we see that the free tropospheric contribution was quite variable, ranging from 0.05 to 0.21, while those within the PBL (altitudes < 2 km) ranged between 0.06 and 0.11. The variations of the AOD and the columnar $å$ are mainly attributed to the different mixed aerosol types arriving over Athens. Furthermore, from the analysis of the back-trajectories of the air masses ending over Athens (not shown here) based on the HYSPLIT code (Draxler and Rolph, 2003), we could identify variable aerosol sources for each day of July, which could play a significant role in the values of the AOD and the columnar $å$ observed. For instance the period 15–20 July was characterized mainly by the presence of anthropogenically produced aerosols over the Balkan Peninsula, whereas the period 20–22 July was characterized by a mixture of anthropogenic and smoke aerosols which originated from the Balkan and the Black Sea greater area, according to HYSPLIT simulations and ATSR satellite data. Finally, on 24–25 July Saharan dust aerosols were advected over the Mediterranean Sea toward Greece.

In Fig. 2, the mean columnar daily values of ω and the real and imaginary part of m are given for 14–28 July, as retrieved by CIMEL. Columnar values of ω (0.87–0.9) and

of the imaginary part of m (0.01–0.02) measured on 21–23 July show the presence of absorptive particles. During THERMOPOLIS concurrent Raman lidar and in situ airborne measurements of aerosol properties were performed between 20 and 25 July (except on 23 July) 2009 over the GAA. In this paper we focus only on the analysis of a case study of nighttime measurements performed in the period 20–21 July, which correspond, as discussed previously, on a mixture of anthropogenic and biomass burning aerosols.

4 Case study 20–21 July 2009

4.1 Measurement situation

During the day of 20 up to early morning hours of 21 July several distinct aerosol layers were observed over the GAA area. Figure 3 shows the temporal evolution of the vertical profile of the range-corrected lidar signal (in arbitrary units) obtained by EOLE at 1064 nm in the 0.3–7-km height range above sea level (a.s.l.) from 08:02 UTC (20 July) to 02:42 UTC (21 July). We see that the aerosols are mainly confined from ground up to 3.5–4 km height, while the PBL reaches 2.3 km height during daytime on 20 July (around 12:45 UTC). The red parts of Fig. 3 (e.g. from 1 km at 08:02 UTC to 2.3 km at 12:45 UTC down to 1.4 km height between 16:30–20:00 UTC; and also aloft from 2.5 to 3.5 km height from 20:00 UTC on 20 July to 02:00 UTC on 21 July) delineate the atmospheric regions with high aerosol backscatter (and hence high aerosol concentrations). Filaments of aerosols are also seen over the daytime PBL on 20 July and over the nocturnal PBL during the late evening hours of 20 July and early morning hours of 21 July, from 2 to 3.5 km height. The vertical lines in Fig. 3 delineate the coincident time windows of the Raman lidar and the airborne in situ aerosol measurements obtained over Athens (11:00–13:00 UTC and 01:00–03:00 UTC).

4.2 Spectral aerosol optical properties

We selected to focus on the lidar data obtained within these two time windows, not only due to the coincidence with the airborne in situ measurements, but also due to the aerosols homogeneous mixing, thus delineating two distinct and intense aerosol layers (one between 2.5 and 3.1 km height a.s.l. at the first time window and the other between 2.2 and 3.2 km height a.s.l. at the second time window). Since the second time window is referring to Raman lidar nighttime measurements, this period has been selected for the retrieval of the aerosol optical and microphysical properties, such as a_{aer}, b_{aer}, LR, $å$, m, r_{eff} and ω, using the inversion algorithm of Müller et al. (1999a), as well as for the application of the ISORROPIA model to retrieve the aerosols chemical composition, which is consistent with the retrieved m and ω values.

Thus, in Fig. 4 we show the nighttime (01:00–02:42 UTC) retrieved vertical profiles of the aerosol optical properties (a_{aer}, b_{aer}, LR and $å$-extinction- and $å$-backscatter-related) obtained by EOLE on 21 July. Based on the a_{aer} profiles the retrieved AOD values at 355 nm and 532 nm were 0.82 and 0.43, respectively, while the LR values at 355 and 532 nm ranged between 60 and 90 sr, from 1.5 to 3.5 km height. As previously discussed, the air mass back-trajectory analysis based on the HYSPLIT model (not shown here) indicated that the aerosol-rich air masses sampled between 2 and 3 km height stagnated over the Balkan and the Black Sea areas for the last 2 days prior to our observations and overpassed biomass burning areas (identified as hot spot areas by ATSR data) where they were probably enriched by locally produced and biomass burning aerosols. This is corroborated by the rather high LR (~58–75 sr) and $å$ values (between 1 and 1.6) found between 2–3 km height (cf. Fig. 4), indicating the presence of mixed rather polluted and small urban-like particles, as similarly observed by Wandinger et al. (2002), Müller et al. (2007), Noh et al. (2007, 2008), Amiridis et al. (2009) and Tesche et al. (2009, 2011).

4.3 Microphysical inversion results

Furthermore, the optical data obtained from the Raman lidar measurements were used to retrieve the aerosol microphysical properties by using an inversion algorithm (Müller et al., 1999a, 2001; Veselovskii et al., 2002; Veselovskii et al., 2005). The aerosol profiles were separated into four layers of about 200 m thickness (in the height range between 1.9 and 2.8 km) based on the relatively stable optical properties within each height range. In our case the required homogeneity of the aerosol layer is corroborated by the stability of the LR and the å values within each selected layer. For the retrieval of the aerosol microphysical properties, we used the mean aerosol backscatter and extinction coefficients within three of the four layers (layer 1: 1.9 ± 0.1 km, layer 2: 2.1 ± 0.1 km, layer 3: 2.4 ± 0.1 km and layer 4: 2.8 ± 0.1 km). The derived particle size and m values have been used for the computation of the ω with a Mie-scattering algorithm, assuming that the mixed smoke and anthropogenic particles can be described as equivalent spheres. The uncertainty of the aerosol microphysical properties retrieved, arise from the errors of the optical input data used as input, as well as those generated by the inversion algorithm used. A search grid of complex refractive indices was applied (ranging from 1.2–1.8 in real part and $0i$–$0.08i$ in imaginary part) and particle size parameters (ranging from 10 nm to 5 mm particle radius) which automatically cause approximation errors (Müller et al., 1999a,b, 2001; Veselovskii et al., 2002, 2005). The uncertainties of the retrieved ω values arise from the uncertainties of the retrieved particle size distributions and the complex refractive indices.

The main aerosol microphysical properties (r_{eff}, m and ω) are derived at the four specific layers on 21 July and presented in Fig. 5. In this figure we see that r_{eff} remained lower than 0.4 ± 0.15 µm. The retrieved refractive index values ranging from 1.45–1.55 (real part) and from $0.015i$–$0.05i$ (imaginary part) indicate the presence of strongly absorbing particles, in full accordance with the retrieved values of ω (ranging between 0.88 at 1.9 km down to 0.63 at 2.8 km height). Taking into account the derived aerosol microphysical properties of the air masses ending around 3 km height

between 01:00–02:42 UTC ($r_{\text{eff}} = 0.4 \pm 0.14\,\mu\text{m}$, $m = 1.557\,(\pm 0.125) + 0.05\,(\pm 0.022)i$ and $\omega = 0.63 \pm 0.11$), the available ATSR data and the air mass origin based on the HYSPLIT model, we have strong indications of mixing of biomass burning aerosols with anthropogenic ones (Wandinger et al., 2002; Müller et al., 2007; Noh et al., 2007, 2008).

The in situ aircraft measurements of the aerosol microphysical properties obtained during THERMOPOLIS, together with the corresponding mean optical and microphysical properties of aerosols derived from the Raman lidar data at selected heights, are shown in Table 1. Missing in situ data are denoted by (–). If we compare the in situ with the retrieved values of the aerosol microphysical properties around 2.8 km height, we see that: the measured value of r_{eff} (0.37 µm) was very close to the retrieved mean value within the aerosol layer ($0.4 \pm 0.14\,\mu\text{m}$); the measured value of ω (0.69 at 500 nm) was very close to the retrieved mean value within the aerosol layer (0.63 ± 0.11 at 532 nm), while, the measured value of m ($1.31 + 0.01i$) was quite different from the retrieved mean value within the aerosol layer ($1.557 + 0.05i$) (Table 1). However, we have to take into account that no change of the value of m with humidity growth was considered in our inversion algorithm which could explain the difference found between the two m values (in situ and lidar-derived).

4.4 Chemical inversion results

The final data set of the aerosol optical and microphysical properties for each selected aerosol layer along with the corresponding potential temperature-relative humidity values derived from local radiosounding at 00:00 UTC (Fig. 6, left panel) and water vapor mixing ratio values obtained by the EOLE Raman lidar (01:00–02:42 UTC) (Fig. 6, right panel) on 21 July 2009, were incorporated into the ISORROPIA II model (Fountoukis and Nenes, 2007) to infer the chemical parameters of the aerosols (e.g. dry chemical composition) that are consistent with the retrieved m and ω values (Table 1). More specifically Table 1 summarizes the mean optical, microphysical and chemical

properties of aerosols derived from a synergy of lidar and in situ aircraft data, as well as inversion models at three selected layers for 21 July 2009 (01:00–02:42 UTC).

For layer 1 (1.9 ± 0.1 km), we derived a chemical composition of about 38–60 % sulfate, 0–20 % organic carbon (OC) and very low content of mineral dust (0–10 %). For layer 2 (2.1 ± 0.1 km), we derived a quite smaller concentration of sulfates (15–50 %), an important increase of OC (0–40 %) and similar levels of the mineral dust content (0–15 %) in comparison to layer 1. Finally, for layer 4 we derived a quite smaller concentration of sulfates (0–30 %), a further increase of OC (0–50 %) and similar levels of mineral dust (0–10 %). Indeed, at this layer we found the biggest concentration values of the OC particles which correlate well with the high values of the aerosol refractive index ($1.56 + 0.05i$) which reflect the tendency of OC to partition to the aerosols phase, under the cooler conditions at higher altitudes (Seinfeld and Pandis, 2008).

Our findings for layer 4 are in full accordance with similar m values corresponding to nearly pure biomass burning particles (Wandinger et al., 2002; Schkolnik et al., 2007) or even better, biomass burning particles mixed with urban haze (Müller et al., 2000, 2006; Noh et al., 2011; Weinzierl et al., 2011). This is corroborated even more by the small ω values (0.63 ± 0.11), the high LR values (65–69 sr) and the presence of sulfate particles, as well as the fact that air masses from the lower part of the PBL (around 20:00 UTC on Fig. 3) are found convected up to 2–3 km height (around 01:00 UTC).

5 Inversion columnar comparisons with sunphotometer data (18–21 July 2009)

For selected days (15–27 July 2009) during of the THERMOPOLIS project we retrieved the mean column values of r_{eff} (Fig. 7, open dots) over the GAA, based on the sunphotometer data. In this figure we see that the mean value of r_{eff} during the selected period ranges from 0.25–0.35 µm (with a standard deviation of the order of 0.07). Additionally, we wanted to compare the mean column values of r_{eff} with those retrieved from Raman lidar data. Therefore, at first, for each of three selected days (18, 20, and 21 July) using EOLE Raman lidar data, we followed the same methodology as described for the

case of 21 July 2009, concerning the retrieval of r_{eff} values at five selected layers from near ground to 3 km height. For these retrieval model runs a grid of complex refractive indices from 1.2 to 1.8 (real part) with a step size of 0.025, and from $0i$ to $0.08i$ (imaginary part) with a step width of $0.003i$, was applied. For these inversions runs we used all the acceptable solutions for the retrieval of the final solutions. To obtain an equivalent "columnar" r_{eff} value from ground up to 3 km height, we averaged the retrieved r_{eff} values at the five layers.

The comparison of the "columnar" r_{eff} values retrieved from our inversion algorithm (for 18, 20 and 21 July) with those derived from the sunphotometer inversion, is presented in Fig. 7. We can clearly see in this figure the very good agreement (within 8–10 %) between the sunphotometer- and the lidar-derived r_{eff} values, which can be mainly attributed to the homogeneous mixing of the particles in the lower troposphere (0–3 km). Finally, in Fig. 8, we present the corresponding columnar mean size distribution as retrieved by sunphotometric measurements over Athens for the period 16–27 July 2009 (the mean size distribution curve is given by the black bold line). We clearly see a bi-modal size distribution of particles having diameters around 0.15 µm (small particles) and around 1.5 µm (large particles which are the dominant ones). In any case, the columnar mean size distribution of particles on 20 July gives a large predominance of the large particles (centered around 1.5 µm) versus the smaller ones (centered around 0.15 µm), in between we find the lidar-derived particles diameters which are of the order of 0.6–0.8 µm in the 2–3 km height region. We also see that the retrieved aerosol extinction-related å – 355/532 nm values ranged from 1.35 to 1.51 (Table 1) are in good accordance with the column mean values (1.45–1.51) derived from the CIMEL data during 20–21 July (Fig. 1, upper panel).

6 Summary and concluding remarks

During THERMOPOLIS concurrent ground-based and aircraft measurements of the aerosol optical and microphysical properties were performed over GAA during July 2009. A novel procedure has been developed to retrieve, simultaneously, the optical, microphysical and chemical properties of aerosols based on the vertical profiles of three aerosol backscatter, two aerosol extinction coefficients and water vapor mixing ratio, all obtained from a 6-wavelength Raman lidar system. Our approach was applied during a case study of selected ground-based Raman lidar data (biomass burning particles mixed with haze) and was successfully compared, on a preliminary basis, to in situ aircraft and sun photometric data, concerning basic aerosol microphysical properties (r_{eff}, ω and m). We found that r_{eff} was 0.3–0.4 µm, ω at 532 nm ranged from 0.63 to 0.88 (decreasing with height) and m ranged from $1.45 + 0.015i$ to $1.56 + 0.05i$, in good accordance with in situ aircraft measurements.

For comparison highly absorbing smoke/urban particles have been reported in previous studies. A summary for different regions on the globe (South America, South India) is given by Müller et al. (2000, 2003, 2005), where real parts of m ranged from 1.5 to 1.66 at visible wavelengths and imaginary parts ranged from $0.01i$ to $0.07i$, in good accordance (within the statistical error) with our retrievals. The imaginary part values of m reported in these references do not show a clear pattern of change of imaginary part with transport time. Murayama et al. (2004) reported values of ω of the order of 0.95 ± 0.06 at 532 nm around the peak of a Siberian forest fire smoke event over Japan, while O'Neill et al. (2002) retrieved values of ω in the ranging 0.97 to 0.99, a distance of 32 km from the biomass burning aerosol sources. Wandinger et al. (2002) found values of ω of 0.76 ± 0.06 and 0.81 ± 0.05 at 355 and 532 nm, respectively, for transport of forest-fire smoke from western Canada, in accordance with Müller et al. (2006). Later, Alados Arboledas et al. (2007) obtained values of ω ranging from 0.80–0.87 (440–1020 nm) for a lofted smoke plume monitored at a high mountain station with sunphotometer. Recently, Alados Arboledas et al. (2011) measured values of ω (0.76–0.9)

depending on the measurement wavelength for the case of fresh smoke pollution over Granada. Müller et al. (2005, 2006) and Noh et al. (2007, 2011) reported on r_{eff} values very close to ours (0.3–0.4 µm) in case of mixed biomass burning and urban haze particles over Germany and Korea. Finally, Müller et al. (2007) reported on *å* and LR values very close to ours (1.35–1.51 and 65–78 sr, respectively) in case of biomass burning and urban haze particles, based on a 10-years database of Raman lidar observations carried out in Europe, Asia and Africa.

The retrieved aerosol chemical composition in the 2–3 km height region, which is consistent with the retrieved m and ω values, gave a variable range of sulfate (0–60 %) and organic carbon (OC) content (0-50%), although the OC content increased (up to 50 %) and the sulfate content dropped (up to 30 %) around 3 km height; in connection with the retrieved low ω value (0.63), it indicates the presence of absorbing biomass burning smoke mixed with urban haze. Finally, the retrieved aerosol microphysical properties (*å* and r_{eff}) were compared with column-integrated sunphotometer data, presenting a good accordance. Our procedure needs to be further tested with in situ aerosol microphysical and chemical aircraft data in the lower troposphere to improve its methodology and further minimize the concurrent retrieval uncertainties.

Acknowledgements. The financial support for EARLINET (EARLINET-ASOS) by the European Commission under grant RICA-025991 is gratefully acknowledged. The financial support for the project THERMOPOLIS by the European Space Agency (ESA-AO/1-5502/07/NL/HE) is also gratefully acknowledged. Air masses back trajectories were produced with the Hybrid Single-Particle Lagrangian Integrated Trajectory model (NOAA). The authors gratefully acknowledge the NOAA Air Resources Laboratory (ARL) for the provision of the HYSPLIT transport and dispersion model. ETK acknowledges internal financial support from Democritus University of Thrace. This research has also been co-financed by the European Union (European Social Fund - ESF) and Greek national funds through the Operational Program "Education and Lifelong Learning" of the National Strategic Reference Framework (NSRF) - Research Funding Program: Heracleitus II, Investing in knowledge society through the European Social Fund. REM acknowledges the funding of the Greek State Scholarship Foundation: IKY. The radiosonde data were provided by the Hellenic National Meteorological Service (HNMS).

References

Adams, P. J. and Seinfeld, J. H.: Predicting global aerosol size distributions in general circulation models, J. Geophys. Res., 104, 13791–13823, doi:10.1029/2001JD001010, 2002.

Alados-Arboledas, L., Guerrero-Rascado, J. L., Lyamani, H., Navas-Guzman, F., and Olmo, F. J.: Characterization of the atmospheric aerosol by combination of Lidar and sun-photometry, Proc. SPIE, 6750, 67500J, doi:10.1117/12.737557, 2007.

Amiridis, V., Balis, D. S., Giannakaki, E., Stohl, A., Kazadzis, S., Koukouli, M. E., and Zanis, P.: Optical characteristics of biomass burning aerosols over Southeastern Europe determined from UV-Raman lidar measurements, Atmos. Chem. Phys., 9, 2431–2440, doi:10.5194/acp-9-2431-2009, 2009.

Ansmann, A., Riebesell, M., Wandinger, U., Weitkamp, C., Voss, C., Lahmann, W., and Michaelis, W.: Combined Raman elastic-backscatter lidar for vertical profiling of moisture, aerosol extinction, backscatter, and lidar ratio, Appl. Phys. B, 55, 18–28, 1992.

Böckmann, C., Wandinger, U., Ansmann, A., Bosenberg, J., Amiridis, V., Boselli, A., Delaval, A., De Tomasi, F., Frioud, M., Grigorov, I., Hagard, A., Horvat, M., Iarlori, M., Komguem, L., Kreipl, S., Larcheveque, G., Matthias, V., Papayannis, A., Pappalardo, G., Rocadenbosch, F., Rodrigues, J. A., Schneider, J., Shcherbakov, V., and Wiegner, M.: Aerosol lidar intercomparisons in the frame of EARLINET: Part II – Aerosol backscatter algorithms, Appl. Optics, 43, 977–989, 2004.

Bösenberg, J., Timm, R., and Wulfmeyer, V.: Study of retrieval algorithms for a backscatter lidar, Final Report, MPI Report No. 226, Hamburg, 1–66, 1997.

Bösenberg, J., Matthias, V., Amodeo, A., Amoiridis, V., Ansmann, A., Baldasano, J. M., Balin, I., Balis, D., Böckmann, C., Boselli, A., Carlsson, G., Chaikovsky, A., Chourdakis, G., Comerón, A., De Tomasi, F., Eixmann, R., Freudenthaler, V., Giehl, H., Grigorov, I., Hågård, A., Iarlori, M., Kirsche, A., Kolarov, G., Komguem, L., Kreipl, S., Kumpf, W., Larchevêque, G., Linné, H., Matthey, R., Mattis, I., Mekler, A., Mironova, I., Mitev, V., Mona, L., Müller, D., Music, S., Nickovic, S., Pandolfi, M., Papayannis, A., Pappalardo, G., Pelon, J., Pérez, C., Perrone, R. M., Persson, R., Resendes, D. P., Rizi, V., Rocadenbosch, F., Rodrigues, J. A., Sauvage, L., Schneidenbach, L., Schumacher, R., Shcherbakov, V., Simeonov, V., Sobolewski, P., Spinelli, N., Stachlewska, I., Stoyanov, D., Trickl, T., Tsaknakis, G., Vaughan, G., Wandinger, U., Wang, X., Wiegner, M., Zavrtanik, M., and Zerefos, C.: EARLINET project: A European Aerosol Research Lidar Network, Contract EVR1-CT1999-40003, Final Report, Hamburg,

1–250, 2003.
Bond, T. C., Anderson, T. L. and Campbell, D.: Calibration and intercomparison of filter based measurements of visible light absorption by aerosols, Aerosol Sci. Tech., 30, 582–600, doi:10.1080/027868299304435, 1999.
Daglis, I., Rapsomanikis, S., Kourtidis, K., Melas, D., Papayannis, A., Keramitsoglou, I., Giannaros, T., Amiridis, V., Petropoulos, G., Sobrino, J., Manunta, P., Grobner, J., Paganini, M., and Bianchi, R.: Mapping The Urban Heat Island Effect In Athens: Results Obtained From The UHI and Thermopolis 2009 Projects, European Geophys. Union, Geophys. Res. Abstr., 12, EGU2010-915-1, 2010.
Draxler, R. R. and Rolph, G. D.: HYSPLIT (HYbrid Single-Particle Lagrangian Integrated Trajectory) Model Access via NOAA ARL READY Website, NOAA Air Resources Laboratory, Silver Spring, MD, 2003.
Dulac, F. and Chazette, P.: Airborne study of a multi-layer aerosol structure in the eastern Mediterranean observed with the airborne polarized lidar ALEX during a STAAARTE campaign (7 June 1997), Atmos. Chem. Phys., 3, 1817–1831, doi:10.5194/acp-3-1817-2003, 2003.
Formenti, P., Boucher, O., Reiner, T., Sprung, D., Andreae, M. O., Wendisch, M., Wex, H., Kindred, D., Tzortziou, M., Vasaras, A., and Zerefos, C.: STAAARTE-MED 1998 summer airborne measurements over the Aegean Sea, 2, Aerosol scattering and absorption, and radiative calculations, J. Geophys. Res., 107, 4451, doi:10.1029/2001JD001536, 2002.
Fountoukis, C. and Nenes, A.: ISORROPIA II: a computationally efficient thermodynamic equilibrium model for $K^+Ca^{2+}Mg^{2+}NH^{4+}Na^+SO_4^{2-}NO_3^-Cl^-H_2O$ aerosols, Atmos. Chem. Phys., 7, 4639–4659, doi:10.5194/acp-7-4639-2007, 2007.
Fountoukis, C., Nenes, A., Sullivan, A., Weber, R., Van Reken, T., Fischer, M., Matías, E., Moya, M., Farmer, D., and Cohen, R. C.: Thermodynamic characterization of Mexico City aerosol during MILAGRO 2006, Atmos. Chem. Phys., 9, 2141–2156, doi:10.5194/acp-9-2141-2009, 2009.
Goody, R. M.: Principles of Atmospheric Physics and Chemistry, Oxford University Press, UK, 1996.
Holben, B. N., Eck, T. F., Slutsker, I., Tanré, D., Buis, J. P., Setzer, A., Vermote, E., Reagan, J. A., Kaufman, Y. J., Nakajima, T., Lavenu, F., Jankowiak, I., and Smirnov, A.: AERONET-A federated instrument network and data archive for aerosol characterization, Remote Sens. Environ., 66, 1–16, doi:10.1016/S0034-4257(98)00031-5, 1998.

Karageorgos, E. T. and Rapsomanikis, S.: Chemical characterization of the inorganic fraction of aerosols and mechanisms of the neutralization of atmospheric acidity in Athens, Greece, Atmos. Chem. Phys., 7, 3015–3033, doi:10.5194/acp-7-3015-2007, 2007.
Karydis, V. A., Tsimpidi, A. P., Fountoukis, C., Nenes, A., Zavala, M., Lei, W., Molina, L. T., and Pandis, S. N.: Simulating the fine and coarse inorganic particulate matter concentrations in a polluted megacity, Atmos. Environ., 44, 608–620, 2010.
Kirkevag, A., Iversen, T., Kristjansson, J. E., Seland, O., and Debernard, J. B.: On the additivity of climate response to anthropogenic aerosols and CO_2, and the enhancement of future global warming by carbonaceous aerosols, Tellus A, 60, 513–527, 2008.
Klett, J.: Lidar Inversion with variable backscatter extinction ratios. Appl. Optics, 24, 1638–1643, 1985.
Lee, S. S.: Dependence of aerosol-precipitation interactions on humidity in a multiple-cloud system, Atmos. Chem. Phys., 11, 2179–2196, doi:10.5194/acp-11-2179-2011, 2011.
Levin, Z. and Cotton, W.: Aerosol Pollution Impact on Precipitation: A Scientific Review, Springer, New York, 2009.
Lohmann, U., Rotstayn, L., Storelvmo, T., Jones, A., Menon, S., Quaas, J., Ekman, A. M. L., Koch, D., and Ruedy, R.: Total aerosol effect: radiative forcing or radiative flux perturbation?, Atmos. Chem. Phys., 10, 3235–3246, doi:10.5194/acp-10-3235-2010, 2010.
Mamouri, R. E., Papayannis, A., Tsaknakis, G., and Amiridis, V.: Six-month ground-based water vapour Raman lidar measurements over Athens, Greece and system validation, J. Optoel. Adv. Mater., 9, 3546–3548, 2007.
Matthias, V., Freudenthaler, V., Amodeo, A., Balin, I., Balis, D., Bösenberg, J., Chaikovsky, A., Chourdakis, G., Comeron, A., Delaval, A., De Tomasi, F., Eixmann, R., Hågård, Ar., Komguem, L., Kreipl, S., Renaud, M., Rizi, V., Rodrigues, J. A., Wandinger, U., and Xuan, W.: Aerosol Lidar Intercomparison in the Framework of the EARLINET Project, 1. Instruments, Appl. Optics, 43, 961–976, 2004a.
Matthias, V., Balis, D., Bösenberg, J., Eixmann, R., Iarlori, M., Komguem, L., Mattis, I., Papayannis, A., Pappalardo, G., Perrone, M. R., and Wang, X.: Vertical aerosol distribution over Europe: Statistical analysis of Raman lidar data from 10 European Aerosol Research Lidar Network (EARLINET) stations, J. Geophys. Res., 109, D18201, doi:10.1029/2004JD004638, 2004b.

Mattis, I., Ansmann, A., Müller, D., Wandinger, U., and Althausen, D.: Dual-wavelength Raman lidar observations of the extinction-to-backscatter ratio of Saharan dust, Geophys. Res. Lett., 29, 1306, doi:10.1029/2002GL014721, 2002.

Metzger, S., Mihalopoulos, N., and Lelieveld, J.: Importance of mineral cations and organics in gas-aerosol partitioning of reactive nitrogen compounds: case study based on MINOS results, Atmos. Chem. Phys., 6, 2549–2567, doi:10.5194/acp-6-2549-2006, 2006.

Mihalopoulos, N., Stephanou, E., Kanakidou, M., Pilitsidis, S., and Bousquet, P.: Tropospheric aerosol ionic composition in the Eastern Mediterranean region, Tellus B, 49, 314–326, 1997.

Moya, M., Ansari, A. S., and Pandis, S. N.: Partitioning of nitrate and ammonium between the gas and particulate phases during the 1997 IMADA-AVER study in Mexico City, Atmos. Environ., 35, 1791–1804, 2001.

Müller, D., Wandinger, U., and Ansmann, A.: Microphysical particle parameters from extinction and backscatter lidar data by inversion with regularization: Theory, Appl. Optics, 38, 2346–2357, 1999a.

Müller, D., Wandinger, U., and Ansmann, A.: Microphysical particle parameters from extinction and backscatter lidar data by inversion with regularization: Simulation, Appl. Optics, 38, 2358–2368, 1999b.

Müller, D., Wagner, F., Althausen, D., Wandinger, U., and Ansmann, A.: Physical properties of the Indian aerosol plume from six-wavelength lidar observations on March 1999 of the Indian Ocean Experiment, Geophys. Res. Lett., 27, 1403–1406, 2000.

Müller, D., Wandinger, U., Althausen, D., and Fiebig, M.: Comprehensive particle characterization from three wavelength Raman-lidar observations: case study, Appl. Optics, 40, 4863–4869, 2001.

Müller, D., Franke, K., Ansmann, A., Althausen, D., and Wagner, F.: Indo-Asian pollution during INDOEX: Microphysical particle properties and single-scattering albedo inferred from multiwavelength lidar observations, J. Geophys. Res., 108, 4600, doi:10.1029/2003JD003538, 2003.

Müller, D., Mattis, I., Wandinger, U., Ansmann, A., Althausen, D., and Stohl, A.: Raman lidar observations of aged Siberian and Canadian forest fire smoke in the free troposphere over Germany in 2003: Microphysical particle characterization, J. Geophys. Res., 110, D17201, doi:10.1029/2004JD005756, 2005.

Müller, D., Tesche, M., Eichler, H., Engelmann, R., Althausen, D., Ansmann, A., Cheng, Y. F., Zhang, Y. H., and Hu, M.: Strong particle light absorption over the Pearl River Delta (south China) and Beijing (north China) determined from combined Raman lidar and Sun photometer observations, Geophys. Res. Lett., 33, L20811, doi:10.1029/2006GL027196, 2006.

Müller, D., Ansmann, A., Mattis, I., Tesche, M., Wandinger, U., Althausen, D., and Pisani, G.: Aerosol-type-dependent lidar ratios observed with Raman lidar, J. Geophys. Res., 112, D16202, doi:10.1029/2006JD008292, 2007.

Murayama, T., Müller, D., Wada, K., Shimizu, A., Sekigushi, M., and Tsukamato, T.: Characterization of Asian dust and Siberian smoke with multi-wavelength Raman lidar over Tokyo, Japan in spring 2003, Geophys. Res. Lett., 31, L23103, doi:10.1029/2004GL021105, 2004.

Noh, Y. M., Kim, Y. J., Choi, B. C., and Murayama, T.: Aerosol lidar ratio characteristics measured by a multi-wavelength Raman lidar system at Anmyeon island, Korea, Atmos. Res., 86, 76–87, doi:10.1016/j.atmosres.2007.03.006, 2007.

Noh, Y. M., Kim, Y. J., and Müller, D.: Seasonal characteristics of lidar ratios measured with a Raman lidar at Gwangju, Korea in spring and autumn, Atmos. Environ., 42, 2208–2224, 2008.

Noh, Y. M., Müller, D., Mattis, I., Lee, H., and Kim, Y. J.: Vertically resolved light-absorption characteristics and the influence of relative humidity on particle properties: Multiwavelength Raman lidar observations of East Asian aerosol types over Korea, J. Geophys. Res., 116, D06206, doi:10.1029/2010JD014873, 2011.

Nowak, J. B., Huey, L. G., Russell, A. G., Tian, D., Neuman, J. A., Orsini, D., Sjostedt, S. J., Sullivan, A. P., Tanner, D. J., Weber, R. J., Nenes, A., Edgerton, E., and Fehsenfeld, F. C.: Analysis of urban gas phase ammonia measurements from the 2002 Atlanta Aerosol Nucleation and Real-Time Characterization Experiment (ANARChE), J. Geophys. Res., 111, D17308, doi:10.1029/2006JD007113, 2006.

O'Neill, N. T., Eck, T. F., Holben, B. N., Smirnov, A., Royer, A., and Li, Z.: Optical properties of boreal forest fire smoke derived from Sun photometry, J. Geophys. Res., 107, 4125, doi:10.1029/2001JD000877, 2002.

Osterloh, L., Böckmann, C., Mamouri, R. E., and Papayannis, A.: An Adaptive Base Point Algorithm for the Retrieval of Aerosol Microphysical Properties, Open Atmos. Sci. J., 5, 61–73, 2011.

Papayannis, A., Balis, D., Amiridis, V., Chourdakis, G., Tsaknakis, G., Zerefos, C., Castanho, A. D. A., Nickovic, S., Kazadzis, S., and Grabowski, J.: Measurements of Saharan dust aerosols over the Eastern Mediterranean using elastic backscatter-Raman lidar, spectrophotometric and satellite observations in the frame of the EARLINET project, Atmos. Chem. Phys., 5, 2065–2079, doi:10.5194/acp-5-2065-2005, 2005.

Papayannis, A., Mamouri, R. E., Remoundaki, E., Bourliva, A., Tsaknakis, G., Amiridis, V., Kokkalis, P., Veselovskii, I., Kolgotin, A., and Samara, C.: Optical, microphysical and chemical properties of Saharan dust aerosols using a multi-wavelength Raman lidar, in situ sensors and modeling, Proc. of the 25th International Laser Radar Conference, 5–9 July 2010, St. Petersburg, Russia, 535–538, 2010.

Papayannis, A., Mamouri, R. E., Amiridis, V., Remoundaki, E., Tsaknakis, G., Kokkalis, P., Veselovskii, I., Kolgotin, A., Nenes, A., and Fountoukis, C.: Optical-microphysical properties of Saharan dust aerosols and composition relationship using a multi-wavelength Raman lidar, in situ sensors and modelling: a case study analysis, Atmos. Chem. Phys. Discuss., 11, 25473–25516, doi:10.5194/acpd-11-25473-2011, 2011.

Pappalardo, G., Amodeo, A., Wandinger, U., Matthias, V., Bösenberg, J., Alpers, M., Amiridis, V., de Tomasi, F., Frioux, M., Iarlori, M., Komguen, L., Larcheveque, G., Papayannis, A., Schumacher, R., and Wang, X.: Aerosol lidar intercomparison in the frame of EARLINET: Part III: Aerosol extinction Raman lidar algorithm intercomparison, Appl. Optics, 43, 5370–5385, 2004.

Pringle, K. J., Tost, H., Message, S., Steil, B., Giannadaki, D., Nenes, A., Fountoukis, C., Stier, P., Vignati, E., and Lelieveld, J.: Description and evaluation of GMXe: a new aerosol submodel for global simulations (v1), Geosci. Model Dev., 3, 391–412, doi:10.5194/gmd-3-391-2010, 2010.

Pye, H. O. T., Liao, H., Wu, S., Mickley, L. J., Jacob, D. J., Henze, D. K., and Seinfeld, J. H.: Effect of changes in climate and emissions on future sulfate-nitrate-ammonium aerosol levels in the United States, J. Geophys. Res., 114, D01205, doi:10.1029/2008JD010701, 2009.

Quaas, J., Ming, Y., Menon, S., Takemura, T., Wang, M., Penner, J. E., Gettelman, A., Lohmann, U., Bellouin, N., Boucher, O., Sayer, A. M., Thomas, G. E., McComiskey, A., Feingold, G., Hoose, C., Kristjánsson, J. E., Liu, X., Balkanski, Y., Donner, L. J., Ginoux, P. A., Stier, P., Grandey, B., Feichter, J., Sednev, I., Bauer, S. E., Koch, D., Grainger, R. G., Kirkevåg, A., Iversen, T., Seland, Ø., Easter, R., Ghan, S. J., Rasch, P. J., Morrison, H., Lamarque, J.-F., Iacono, M. J., Kinne, S., and Schulz, M.: Aerosol indirect effects – general circulation

model intercomparison and evaluation with satellite data, Atmos. Chem. Phys., 9, 8697–8717, doi:10.5194/acp-9-8697-2009, 2009.

Ramanathan, V. and Feng, Y.: Air pollution, greenhouse gases and climate change: Global and regional perspectives, Atmos. Environ., 43, 37–50, 2009.

Rapsomanikis, S., Kelektsoglou, K., Karageorgos, E. T., and Kosmadakis, I.: Indirect aerosol forcing of climate over the South Eastern Mediterranean urban environment, Int. J. Remote Sens., 33, 1–20, 2011.

Remoundaki, E., Bourliva, A., Kokkalis, P., Mamouri, R. E., Papayannis, A., Grigoratos, T., Samara, C., and Tsezos, M.: Composition of PM_{10} during a Saharan dust transport event over Athens, Greece, Sci. Total Environ., 409, 4361–4372, 2011.

San Martini, F. M., Dunlea, E. J., Volkamer, R., Onasch, T. B., Jayne, J. T., Canagaratna, M. R., Worsnop, D. R., Kolb, C. E., Shorter, J. H., Herndon, S. C., Zahniser, M. S., Salcedo, D., Dzepina, K., Jimenez, J. L., Ortega, J. M., Johnson, K. S., McRae, G. J., Molina, L. T., and Molina, M. J.: Implementation of a Markov Chain Monte Carlo method to inorganic aerosol modeling of observations from the MCMA-2003 campaign – Part II: Model application to the CENICA, Pedregal and Santa Ana sites, Atmos. Chem. Phys., 6, 4889–4904, doi:10.5194/acp-6-4889-2006, 2006.

Schkolnik, G., Chand, D., Hoffer, A., Andreae, M. O., Erlick, C., Swietlicki, E., and Rudic, Y.: Constraining the density and complex refractive index of elemental and organic carbon in biomass burning aerosol using optical and chemical measurements, Atmos. Environ., 41, 1107–1118, 2007.

Stock, M., Cheng, Y. F., Birmili, W., Massling, A., Wehner, B., Müller, T., Leinert, S., Kalivitis, N., Mihalopoulos, N., and Wiedensohler, A.: Hygroscopic properties of atmospheric aerosol particles over the Eastern Mediterranean: implications for regional direct radiative forcing under clean and polluted conditions, Atmos. Chem. Phys., 11, 4251–4271, doi:10.5194/acp-11-4251-2011, 2011.

Tesche, M., Ansmann, A., Müller, D., Althausen, D., Engelmann, R., Freudenthaler, V., and Groß, S.: Vertically resolved separation of dust and smoke over Cape Verde using multiwavelength Raman and polarization lidars during Saharan Mineral Dust Experiment 2008, J. Geophys. Res., 114, D13202, doi:10.1029/2009JD011862, 2009.

Tesche, M., Gross, S., Ansmnann, A., Müller, D., Althausen, D., Freudenthaler, V., and Esselborn, M.: Profiling of Saharan dust and biomass-burning smoke with multiwavelength polarization Raman lidar at Cape Verde, Tellus B, 63, 649–676, 2011.

Veselovskii, I., Kolgotin, A., Griaznov, V., Müller, D., Wandinger, U., and Whiteman, D. N.: Inversion with regularization for the retrieval of tropospheric aerosol parameters from multiwavelength lidar sounding, Appl. Optics, 41, 3685–3699, 2002.

Veselovskii, I., Kolgotin, A., Müller, D., and Whiteman, D. N.: Information content of multiwavelength lidar data with respect to microphysical particle properties derived from eigenvalue analysis, Appl. Optics, 44, 5292–5303, 2005.

Volkert, H., Weckwerth, T., Wernli, H., Wieser, A., and Wirth, M.: The Convective and Orographically-induced Precipitation Study (COPS): The scientific strategy, the field phase, and research highlights, Q. J. Roy. Meteorol. Soc., 137, 3–30, doi:10.1002/qj.752, 2011.

Wandinger, U., Müller, D., Bockmann, C., Althausen, D., Matthias, V., Bösenberg, J., Weiss, V., Fiebig, M., Wendisch, M., Stohl, A., and Ansmann, A.: Optical and microphysical characterization of biomass-burning and industrial-pollution aerosols from multiwavelength lidar and aircraft measurements, J. Geophys. Res., 107, 8125, doi:10.1029/2000JD000202, 2002.

Weinzierl, B., Sauer, D., Esselborn, M., Petzold, A., Veira, A., Rose, M., Mund, S., Wirth, M., Ansmann, A., Tesche, M., Gross, S., and Freudenthaler, V.: Microphysical and optical properties of dust and tropical biomass burning aerosol layers in the Cape Verde region-an overview of the airborne in situ and lidar measurements during SAMUM-2, Tellus B, 63, 589–618, 2011.

Weitkamp, C.: Lidar: Range-Resolved Optical Remote Sensing of the Atmosphere, Springer Science, NY, USA, 2005.

Wulfmeyer, V., Behrendt, A., Kottmeier, C., Corsmeier, U., Barthlott, C., Craig, G. C., Hagen, M., Althausen, D., Aoshima, F., Arpagaus, M., Bauer, H.-S., Bennett, L., Blyth, A., Brandau, C., Champollion, C., Crewell, S., Dick, G., Di Girolamo, P., Dorninger, M., Dufournet, Y., Eigenmann, R., Engelmann, R., Flamant, C., Foken, T., Gorgas, T., Grzeschik, M., Handwerker, J., Hauck, C., Höller, H., Junkermann, W., Kalthoff, N., Kiemle, C., Klink, S., König, M., Krauss, L., Long, C. N., Madonna, F., Mobbs, S., Neininger, B., Pal, S., Peters, G., Pigeon, G., Richard, E., Rotach, M. W., Russchenberg, H., Schwitalla, T., Smith, V., Steinacker, R., Trentmann, J., Turner, D. D., van Baelen, J., and Vogt, S.: The Convective and Orographically-induced Precipitation Study (COPS): the scientific strategy, the field phase, and research highlights, Q. J. Roy. Meteorol. Soc., 137, 3–30, 2011.

Wyser, K.: The effective radius in large-scale models: impact of aerosols and coalescence, Atmos. Res., 49, 213–234, 1998.

Yu, S., Dennis, R., Roselle, S., Nenes, A., Walker, J., Eder, B., Schere, K., Swall, J., and Robarge, W.: An assessment of the ability of three-dimensional air quality models with current thermodynamic equilibrium models to predict aerosol NO^{-3}, J. Geophys. Res., 110, D07S13, doi:10.1029/2004JD004718, 2005.

Zhang, J., Chameides, W. L., Weber, R., Cass, G., Orsini, D., Edgerton, E. S., Jongejan, P., and Slanina, J.: An evaluation of the thermodynamic equilibrium assumption for fine particulate composition: Nitrate and ammonium during the 1999 Atlanta Supersite Experiment, J. Geophys. Res., 107, 8414, doi:10.1029/2001JD001592, 2003.

Table 1. Mean aerosol optical, microphysical and chemical properties derived from a synergy of lidar and in situ aircraft data, as well as inversion models.

Height a.s.l. [km]	á [$\alpha_{355}/\alpha_{532}$] lidar	LR_{355} [sr] lidar	LR_{532} [sr] lidar	r_{eff} [µm] lidar	r_{eff} [µm] in situ	ω_{532} lidar	ω_{500} in situ	m lidar	m in situ	Chemical composition – Relative humidity [%] Sulfate	Organic carbon	Dust	RH
1.9 ± 0.1	1.51 ± 0.05	78 ± 2	72 ± 1	0.3 ± 0.15	–	0.88 ± 0.08	–	1.45 + 0.015*i*	–	38–60	0–20	0–10	60
2.1 ± 0.1	1.38 ± 0.01	72 ± 1	66 ± 1	0.33 ± 0.14	–	0.85 ± 0.1	–	1.47 + 0.019*i*	–	15–50	0–40	0–15	68
2.8 ± 0.1	1.35 ± 0.02	69 ± 0.7	65 ± 1	0.4 ± 0.14	0.37	0.63 ± 0.11	0.698	1.56 + 0.051*i*	1.31 + 0.01*i*	0–30	0–50	0–10	91

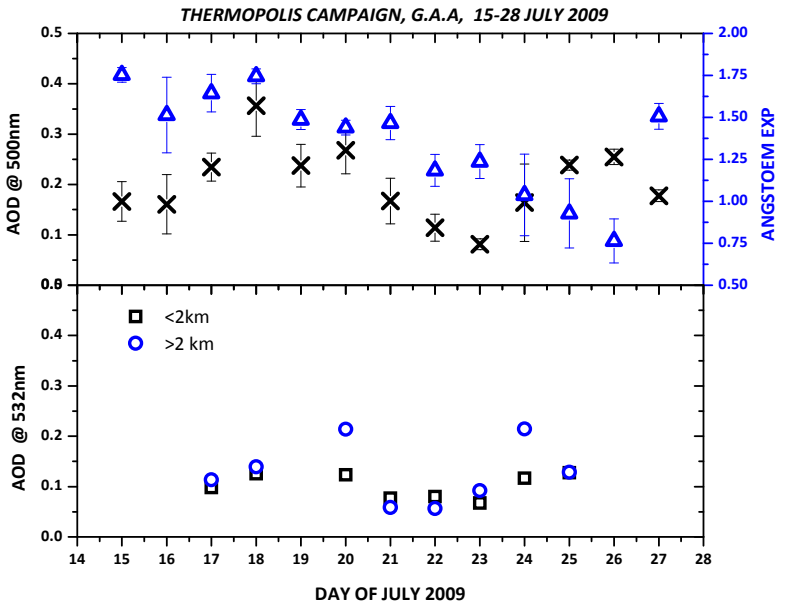

Fig. 1. Upper panel: AOD (crosses) and Ångström exponent (triangles) derived by sunphotometer over Athens from 15–27 July 2009; lower panel: AOD below (squares) and above (open dots) 2 km height derived by Raman lidar measurements in the period 17–27 July 2009 (except on 19 July 2009).

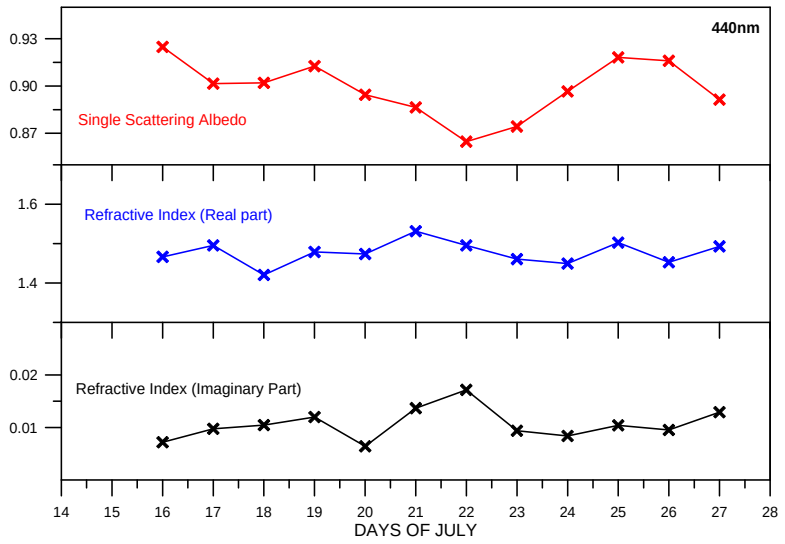

Fig. 2. Top panel: single scattering albedo (ω); middle and lower panel, respectively: real and imaginary part of refractive Index (m) measured by sunphotometer at 440 nm over Athens for the time period 15–27 July 2009.

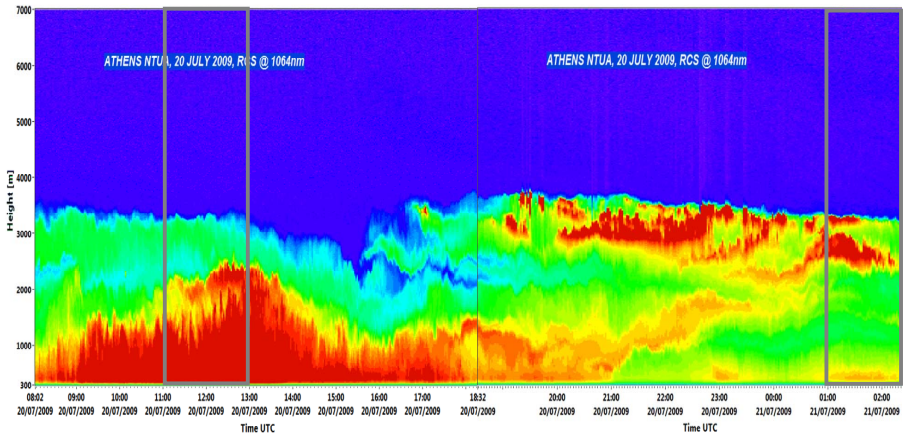

Fig. 3. Temporal evolution of the range-corrected lidar signal (RCS) obtained over Athens at 1064 nm, between 08:02 UTC (20 July 2009) and 02:42 UTC (21 July 2009). The grey panels refer to the aircraft flight periods.

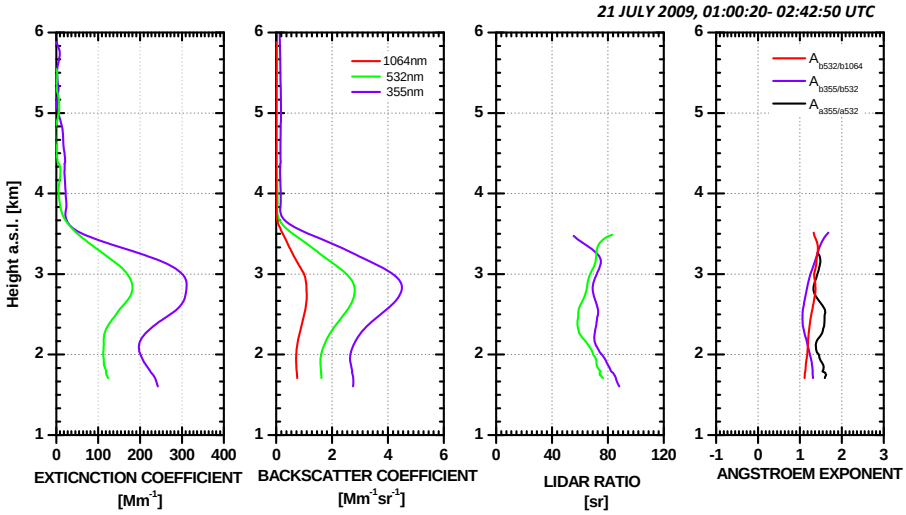

Fig. 4. Vertical profiles of the aerosol optical parameters (extinction, backscatter, lidar ratio, Ångström exponent) retrieved by the EOLE Raman lidar measurements on 21 July 2009 (01:20–02:42 UTC).

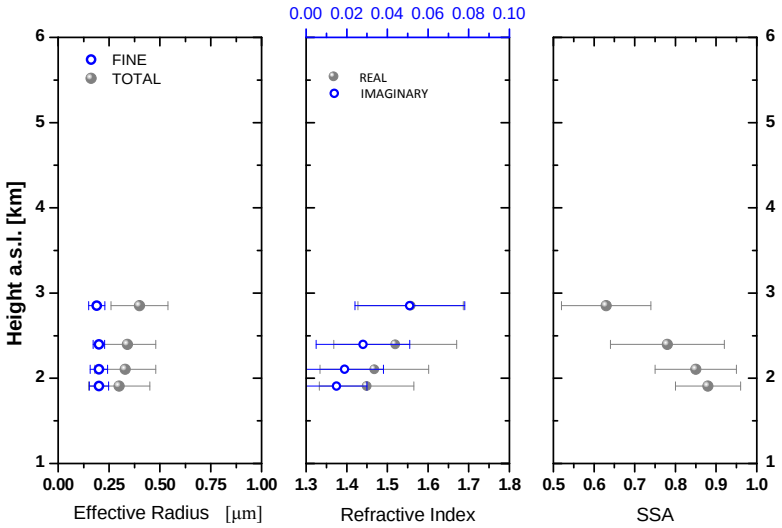

Fig. 5. Retrieved aerosol effective radius (r_{eff}), refractive index (m) and single scattering albedo (ω) based on the aerosol optical properties derived by the EOLE Raman lidar on 21 July 2009.

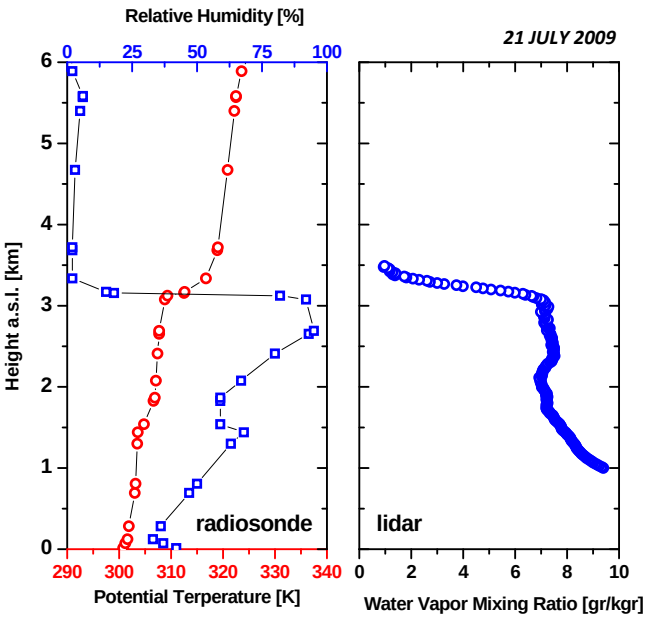

Fig. 6. Potential temperature (K) and relative humidity-RH (%) vertical profiles obtained from radiosonde data on 21 July 2009 (00:00 UTC) (left panel) and water vapor mixing ratio derived from the EOLE Raman lidar measurements on 21 July 2009 (01:20–02:42 UTC).

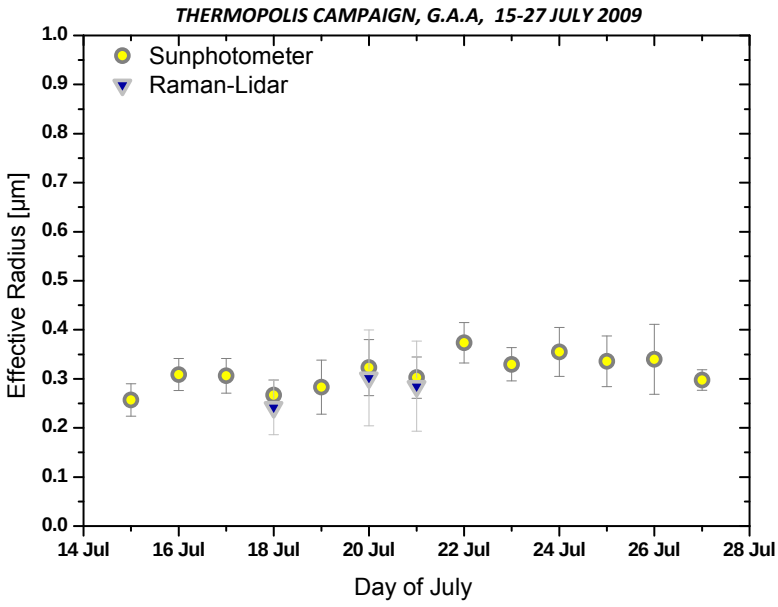

Fig. 7. Total effective radius retrieved from sunphotometer and Raman lidar signal inversions.

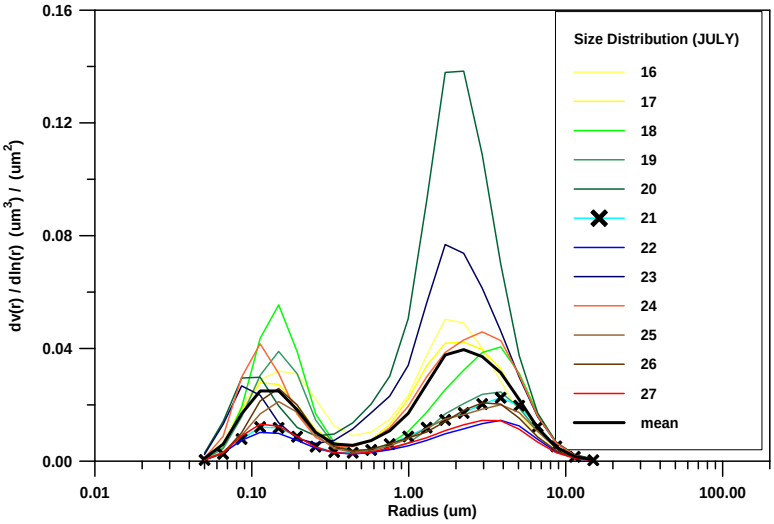

Fig. 8. Mean daily size distribution derived from sunphotometer data over Athens for the period 18–27 July 2009. The cross mark denotes the studied day (21 July 2009).